151

EXPERIMENTAL INVESTIGATION OF DYNAMIC STALL PERFORMANCE FOR THE EDI-M109 AND EDI-M112 AIRFOILS

A.D. GARDNER[*], K. RICHTER[†], H. MAI[‡], A.R.M. ALTMIKUS[§], A. KLEIN[¶] AND C.-H. ROHARDT[‖]

ABSTRACT

An experimental investigation of the dynamic performance of two new rotor blade airfoils was undertaken in a transonic wind tunnel. The EDI-M109 and EDI-M112 airfoils were tested at $0.3 \leq M \leq 0.5$ for pitching motions with amplitude $0.5^\circ \leq \alpha_\pm \leq 8^\circ$ and frequencies $3.3\,\text{Hz} \leq f \leq 45\,\text{Hz}$. The results show that both new airfoils have acceptable dynamic stall performance, and the effect of frequency, amplitude, and higher order pitching motion on these results is described. The pitching moment peak size was found to have an approximately linear correlation to the normalised mean angular velocity, and thus test cases with the same maximum angle of attack and oscillation frequency had similar dynamic stall qualities. The correlation between low aerodynamic damping for high frequency, low amplitude pitching motion and poor dynamic stall performance is shown to be low. The dynamic stall response of the EDI-M112 airfoil is shown to be better for M=0.3 and M=0.4, and the response of the EDI-M109 airfoil is better at M=0.5. The dynamic performance of the airfoils is compared to the OA209.

NOMENCLATURE

$\overline{\alpha'}$	Mean angular velocity [°/second]
α, $\overline{\alpha}$	Angle of attack, mean angle of attack [°]
$\alpha_\pm$	Sinusoidal motion amplitude [°]
$\alpha_{C_{L_{max}},stat}$	α at maximum lift for a static polar [°]
$\overline{\alpha'_{norm}}$	Normalised mean angular velocity
b	Airfoil model breadth (=997 mm)
c	Airfoil chord (=300 mm)
C_L, $\overline{C_L}$, C_{L_p}	Lift coefficient; mean; peak
C_D, $\overline{C_D}$, C_{D_p}	Drag coefficient; mean; peak
C_{my}, $\overline{C_{my}}$, C_{my_p}	Pitching moment coefficient; mean; peak
d	Airfoil thickness [mm]
D	Damping coefficient
f	Frequency [Hz]
M	Mach number
Re	Reynolds number
t	Time [seconds]
v_∞	Freestream flow velocity [m/s]
ω^*	Reduced frequency: ω^*: $\omega^* = 2\pi f c / v_\infty$

[*]Corresponding Author. German Aerospace Center (DLR), Institute of Aerodynamics and Flow Technology (AS), Bunsenstrasse 10, 37073 Göttingen, Germany. *tony.gardner@dlr.de*

[†]DLR-AS

[‡]DLR Institute of Aeroelasticity

[§]Eurocopter Deutschland ETGA

[¶]University of Stuttgart, Institute for Aerodynamics and Gas Dynamics

[‖]DLR-AS

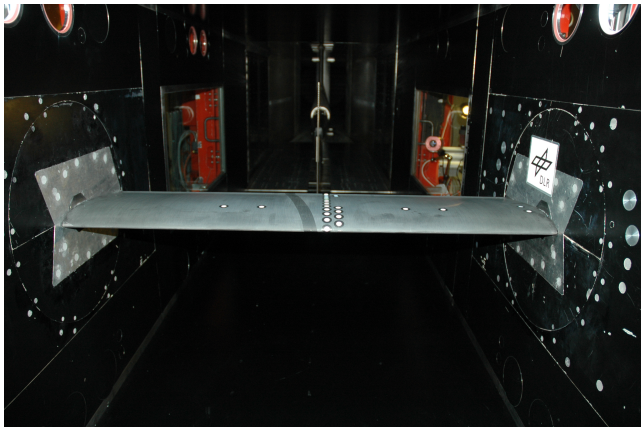

Figure 1: The EDI-M112 airfoil model installed in the test section of the DNW-TWG wind tunnel.

INTRODUCTION

The design of helicopter airfoils has changed in recent years to rely more strongly on numerical prediction of both the dynamic and static properties of potential airfoil designs. Due to problems with the accuracy of prediction models for the dynamic properties of airfoils, and in particular for dynamic stall, experimental investigations are still required to assess the dynamic performance of airfoils. As part of the German Luftfahrtforschungsprogramm (LuFo IV), the German Aerospace Center, University of Stuttgart and Eurocopter Deutschland had a cooperation called INROS to design and evaluate new helicopter airfoils to have good dynamic characteristics at dynamic stall (see also [2]). Two new airfoils were designed for the main rotor of a helicopter with maximum thickness d/c=9% and d/c=12%, and these were designated EDI-M109 and EDI-M112 respectively. The use of unsteady criteria for the design is described by Klein *et al* [3]. This paper investigates selected experimental results illustrating the dynamic performance of the new airfoil.

EXPERIMENTAL ARRANGEMENT

Carbon fibre models with a chord length c=300 mm and a breadth b=997 mm were produced for the 1 m x 1 m adaptive wall test section of the Transonic Wind Tunnel Göttingen (DNW-TWG). The adaptive test section has flexible top and bottom walls which can be adapted to minimise the interference velocities at the wall at the mean angle of attack

of the model. The models are mounted horizontally in the test section (Figure 1) and are driven with pitch-oscillations from shafts through the side-walls attached at the $\frac{1}{4}c$. Hydraulic motors drive the model from both sides and are located outside the test section. The model could be driven in a $\Delta\alpha$=20° range without opening the tunnel, and mean angular velocities $\overline{\alpha'} \leq$200°/sec could be used with sinusoidal movement. The models were each fitted with 48 Kulite unsteady pressure sensors (type XCQ-093) on the centerline, situated so as to guarantee a maximum discretisation error of 1% in lift, pressure-drag and pitching moment computed from the pressure taps during static measurements and dynamic stall. The angle of attack was measured using four high-frequency laser rangefinders on beams attached to each end of the model. A phase-locked data acquisition system, sampled each sensor with 1024 points per period for 160 periods. Data shown here is phase-averaged, showing the mean for each phase point and the standard deviation for every eighth phase point.

The dynamic test points were produced for two classes of points, both with sinusoidal pitching motion about a mean angle: $\alpha = \overline{\alpha} + \alpha_{\pm}\sin(2\pi ft)$ at $M \in$[0.3, 0.4, 0.5] and with Reynolds numbers $4\times10^6 \leq Re/M \leq 7\times10^6$. Points were taken with large amplitudes $4^\circ \leq \alpha_{\pm} \leq 10^\circ$ and low frequency 3.3 Hz$\leq f \leq$6.6 Hz, to generate dynamic stall matching the main rotor rotation rate. A listing of the dynamic stall points used in this paper is in Table 1. In addition, points with low amplitude $0.5^\circ \leq \alpha_{\pm} \leq 2^\circ$ and high frequency 13 Hz$\leq f \leq$45 Hz were tested to produce data for the Liiva criterion [4] for dynamic stall strength.

The experimental data for the EDI-M109, EDI-M112 and OA209 is presented with angle of attack uncorrected for wind tunnel effects, geometry changes in the model compared to the nominal airfoil or other effects. It should be noted that the experimental OA209 geometry used was built in the design shape rather than the industrial shape. The EDI-M109 and EDI-M112 models are designed so that at M=0.8, Re=5.8×10^6 and with maximum lift, the airfoil has a maximum contour deformation of 0.15 mm.

DATA AVERAGING

Variables were phase averaged over 160 cycles of 1024 points to get a mean and standard deviation for each point on the cycle. The standard deviation in α, $\sigma\alpha \leq 0.05^\circ$, and so is not plotted in this paper. Additionally, the mean lift $\overline{C_L}$, mean drag $\overline{C_D}$ and mean pitching moment $\overline{C_{my}}$ over a cycle were taken for each dynamic point by averaging the data over all cycles. The peak lift C_{L_p}, peak drag C_{D_p} and peak pitching moment C_{my_p} were found by analysing the phase-averaged data and finding the maximum value for lift and drag or the minimum value for pitching moment.

The damping coefficient D gives an indication of whether a negative damping will be too large to be counteracted by the structural damping and is computed from the theoretical and measured values of the aerodynamic damping[4]: $D = [-\oint C_{my}\, d\alpha(\alpha_{\pm})^2\pi^3 cf]/[2v_\infty]$, where D=1 for small oscillations with attached flow. This analysis was performed for each dynamic point measured, using the uniform INROS analysis code shared by ECD, Onera, University of Stuttgart and DLR. The damping was additionally computed for the separated modes 1/rev to 6/rev.

$\overline{\alpha}$ [°]	$\alpha_{\pm}$ [°]	C_{L_p} [-]	$\overline{C_L}$ [-]	C_{my_p} [-]	f [Hz]	$\overline{\alpha'}$ [°/s]	ω^* [-]
EDI-M109 at M=0.3, Re=1.2×10^6							
13	7	1.660	1.069	-0.270	5.6	157	0.10
EDI-M109 at M=0.3, Re=1.8×10^6							
10	4	1.500	1.121	-0.116	6.6	106	0.12
10	5	1.569	1.050	-0.220	6.6	132	0.12
10	6	1.652	0.989	-0.252	6.6	158	0.12
10	7	1.679	0.947	-0.282	6.6	185	0.12
11	7	1.588	0.985	-0.207	3.3	92	0.06
11	7	1.639	0.972	-0.257	5.0	140	0.09
11	7	1.686	0.989	-0.285	6.6	185	0.12
12	4	1.592	1.148	-0.233	6.6	106	0.12
12	7	1.692	1.045	-0.295	6.6	185	0.12
EDI-M109 at M=0.3, Re=1.8×10^6 - Dual sine							
12	7	1.699	1.064	-0.306	6.6	185	0.12
EDI-M109 at M=0.4, Re=2.4×10^6							
10	4	1.467	1.130	-0.121	6.6	106	0.09
10	5	1.547	1.076	-0.153	6.6	132	0.09
10	6	1.571	1.016	-0.183	6.6	158	0.09
10	7	1.591	0.969	-0.220	6.6	185	0.09
EDI-M109 at M=0.5, Re=3.0×10^6							
10	4	1.351	1.130	-0.081	6.6	106	0.07
10	5	1.375	1.089	-0.083	6.6	132	0.07
10	6	1.399	1.046	-0.101	6.6	158	0.07
10	7	1.424	1.002	-0.119	6.6	185	0.07
EDI-M109 at M=0.3, Re=1.2×10^6							
13	7	1.690	1.095	-0.1780	5.6	157	0.10
EDI-M112 at M=0.3, Re=1.8×10^6							
8	8	1.687	0.865	-0.133	6.6	211	0.12
10	4	1.546	1.181	-0.026	6.6	106	0.12
10	5	1.597	1.100	-0.090	6.6	132	0.12
10	6	1.653	1.051	-0.134	6.6	158	0.12
10	7	1.711	1.007	-0.175	6.6	185	0.12
11	7	1.452	0.923	-0.168	3.3	92	0.06
11	7	1.543	0.940	-0.186	5.0	140	0.09
11	7	1.621	0.955	-0.209	6.6	185	0.12
12	4	1.616	1.210	-0.135	6.6	106	0.12
12	7	1.781	1.089	-0.233	6.6	185	0.12
EDI-M112 at M=0.3, Re=1.8×10^6 - Dual sine							
12	7	1.868	1.137	-0.290	6.6	185	0.12
EDI-M112 at M=0.4, Re=2.4×10^6							
10	7	1.589	0.894	-0.189	6.6	185	0.12

Table 1: Dynamic airfoil data.

VARIATION OF AMPLITUDE

The primary effect of increasing the amplitude is to increase the severity of the dynamic stall while leaving the type of the stall unchanged. Figures 2 and 3 illustrate the effect of varying the oscillation amplitude for the EDI-M109 and EDI-M112 airfoils respectively. In each case the oscillation frequency was f=6.6 Hz, but of necessity these will have different mean angular velocities (Table 1).

Figure 2 shows the EDI-M109 at a mean angle of α=10° at M=0.3. As the amplitude increases from $\alpha_{\pm}$=4° to $\alpha_{\pm}$7°, the peak lift increases from C_{L_p}=1.500 to C_{L_p}=1.679, but the mean lift over one cycle decreases from $\overline{C_L}$=1.121 to $\overline{C_L}$=0.947 (Table 1). This is typical of dynamic stall, and

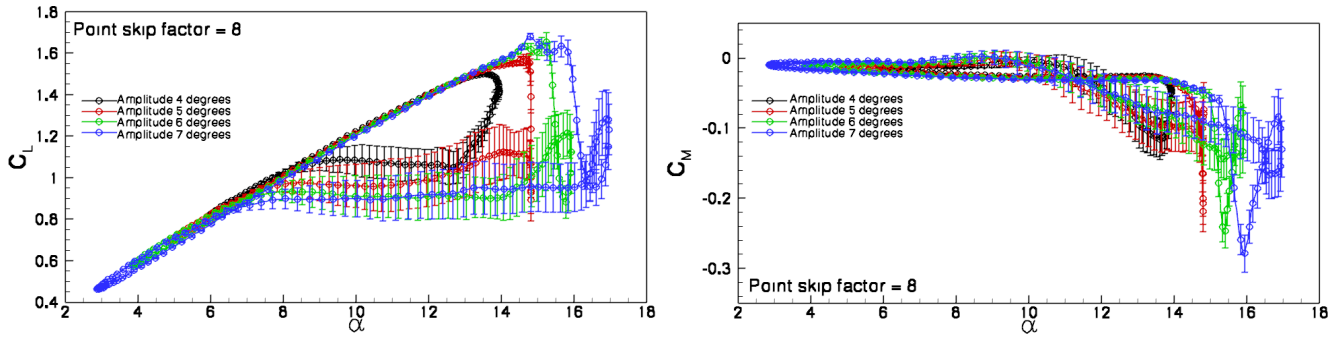

Figure 2: Comparison of lift (Left) and pitching moment coefficient (Right) for the EDI-M109 airfoil with various amplitudes at M=0.3, Re=1.8e6, f=6.6 Hz, α=10±4-7°.

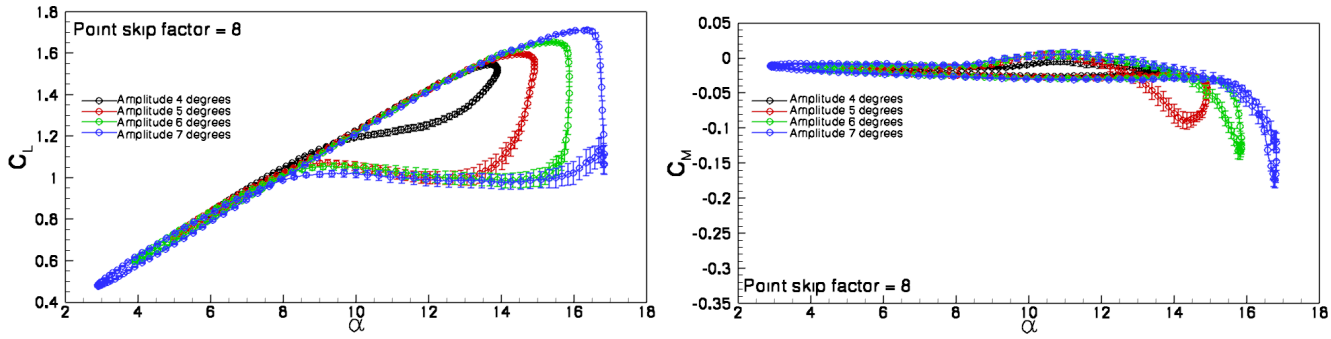

Figure 3: Comparison of lift (Left) and pitching moment coefficient (Right) for the EDI-M112 airfoil with various amplitudes at M=0.3, Re=1.8e6, f=6.6 Hz, α=10±4-7°.

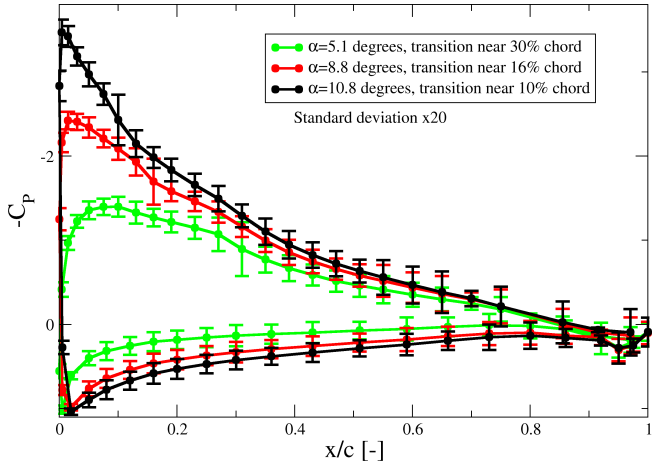

Figure 4: Time sequence of pressure distributions for the EDI-M112 airfoil at M=0.3, Re=1.8e6, f=6.6 Hz, α=10±6°, showing the movement of the transition position.

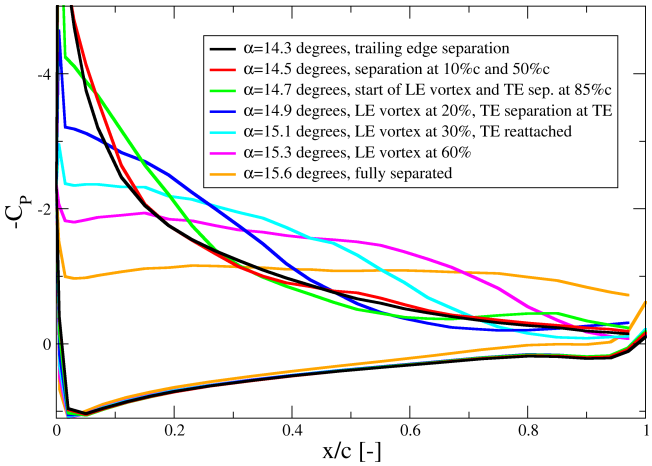

Figure 5: Time sequence of pressure distributions for the EDI-M109 airfoil at M=0.3, Re=1.8e6, f=6.6 Hz, α=10±7°, showing leading edge separation.

there is a corresponding increase in the mean drag over one cycle as the amplitude increases. Similarly, the pitching moment peak increases as the dynamic stall is strengthened at increasing amplitudes from C_{my_p}=-0.116 to C_{my_p}-0.282.

The transition point on the top of the airfoil can be detected from the pressure distributions, as shown in Figure 4, by observing the motion of the pressure step and the increased cycle-to-cycle variation which moves forward as the angle of attack increases. From static polars, where an infrared camera was used to measure the heat flux on both airfoils, we know that this combination is associated with transition over a laminar boundary layer separation. The approximate angle at which the transition reaches the leading edge can be estimated from a time-series of pressure distributions.

For the EDI-M109 at a mean angle of α=10° at M=0.3, the boundary layer transition on the top of the airfoil moves forward on the upstroke reaching the leading edge at around α=10°. There is a reduction in slope of the lift curve at this point, which may or may not be associated with the halting of the transition point movement. The EDI-M109 sees a significant increase in the cycle-to-cycle variation in the pressure signals near the trailing edge above α=13°, and by α=13.5° this has developed into a trailing edge stall. As seen in Figure 5, for the case α=10±7°, by α=14.3° the trailing edge stall is clearly visible and the pressure coefficient on the trailing edge is less than zero. At α=14.5°, the flow separates at 10% and 50% chord, and by α=14.7°, the leading edge vortex has started to move backward. From

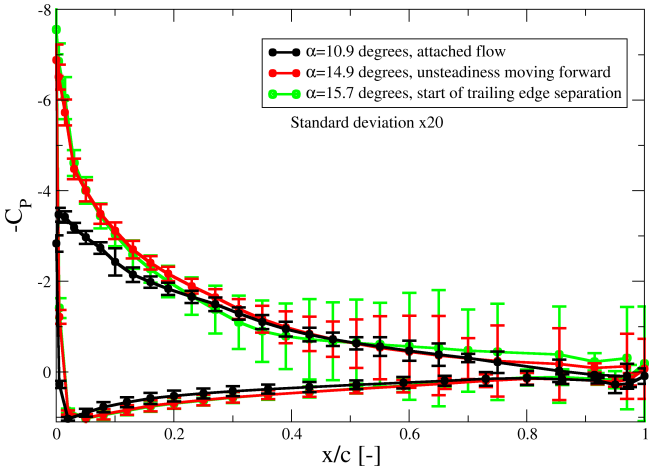

Figure 6: Time sequence of pressure distributions for the EDI-M112 airfoil at M=0.3, Re=1.8e6, f=6.6 Hz, α=10$\pm$7°, showing trailing edge separation.

this point, the aerodynamics is much more like a leading edge separation, since the leading edge stall vortex travels backward, pushing the trailing edge separation off the end of the airfoil. The two peaks in the lift curve for α=10$\pm$7° in Figure 2 at α=14.7° and α=15.8° are associated with the formation of the stall vortex at the leading edge, and with the passage of the stall vortex over the trailing edge. As the stall vortex moves toward the trailing edge, the pitching moment decreases toward a negative peak and at the point where the vortex crosses the trailing edge, the minimum pitching moment is reached. After stall a highly unsteady flow is observed, with reattachment at lower α for higher amplitudes. The pressure distributions show that for the EDI-M109 at M=0.3, the reattachment starts at the trailing edge and moves forward, with the suction peak being the last place to reattach.

Figure 3 shows the EDI-M112 at a mean angle of α=10° at M=0.3. As amplitude increases from $\alpha_{\pm}$=4° to $\alpha_{\pm}$7°, the peak lift increases from C_{L_p}=1.546 to C_{L_p}=1.711 and the mean lift over one cycle decreases from $\overline{C_L}$=1.181 to $\overline{C_L}$=1.007 in the same way as for the EDI-M109 (Table 1). Also similarly, the mean drag over one cycle increases as the amplitude increases, and the pitching moment peak increases from C_{my_p}=-0.036 to C_{my_p}=-0.175. The dynamic stall peaks for the pitching moment are significantly less than for the EDI-M109 at these flow and motion conditions. On the upstroke, the boundary layer transition reaches the leading edge at around α=13°, and at the same angle the pressure signals near the trailing edge start to increase in cycle-to-cycle variation, and the start of the region of unsteady signals moves forward with increasing α. As seen in Figure 6, for the case α=10$\pm$7°, by α=14.9° there is a clear trailing edge separation, which moves slowly forward on the airfoil until the leading edge is reached. For amplitudes of $\alpha_{\pm}$=5° and above, the trailing edge separation is followed by unsteady separated flow. The cycle-to-cycle variation in the lift coefficient in the separated region is significantly less than for the EDI-M109. As for the EDI-M109, the higher amplitudes reattach at lower α, but the difference between different amplitudes is reduced. At $\alpha_{\pm}$=4° there is unsteady flow and a significant hysteresis on the top of airfoil, but a full separation of the flow does not occur. The pressure distributions show that for the EDI-M112 at M=0.3, the reattachment starts at the leading edge and moves backward, with the trailing edge being the last place to reattach.

For the EDI-M109 at M=0.4 (Figure 7) at a mean angle of α=10°, the reduced frequency has reduced to ω^*=0.09 for the constant absolute frequency of f=6.6 Hz (Table 1). As the amplitude increases from $\alpha_{\pm}$=4° to $\alpha_{\pm}$7°, the peak lift increases from C_{L_p}=1.467 to C_{L_p}=1.591. As for M=0.3, as the amplitude increases, the mean lift over one cycle decreases $\overline{C_L}$=1.130 to $\overline{C_L}$=0.969. Similarly to M=0.3, the pitching moment peak increases as the dynamic stall is strengthened at increasing amplitudes from C_{my_p}=-0.121 to C_{my_p}=-0.220. The boundary layer transition on the top of the airfoil reaches the leading edge at around α=9°, and the sudden change in the slope of the lift curves at α=12° is associated with the release of a leading edge stall vortex travelling downstream. The flow in the suction peak is supersonic, and although shock-induced stall is suspected, no strong shock is visible in the pressure distributions. For the EDI-M112 at this flow condition (not shown), the curves look very similar to Figure 3. A single curve at this condition is in Figure 21. In this case the pressure distributions show a strong shock at around 10% chord, followed by separated flow to the trailing edge, leading to trailing edge stall. At M=0.4 the EDI-M109 reattaches from the trailing edge, with the last attachment in the supersonic region, and the EDI-M112 has reattachment from the leading edge.

For M=0.5 (Figure 8) the results change, and there is not the same loss of lift after separation as seen for M=0.3 and M=0.4. For M=0.3 a 16% reduction in mean lift was observed between the minimum and maximum amplitudes, but here the reduction is 11%. After stall no discrete peaks are formed, but the flow has a high cycle to cycle variation in the lift. There is still an increase in the peak lift from C_{L_p}=1.351 to C_{L_p}=1.424 as amplitude increases from $\alpha_{\pm}$=4° to $\alpha_{\pm}$7°, a decrease in mean lift from $\overline{C_L}$=1.130 to $\overline{C_L}$=1.002, and an increase in the pitching moment peak from C_{my_p}=-0.081 to C_{my_p}=-0.119 (Table 1). For the EDI-M109, the boundary layer transition reaches the leading edge at around α=7° on the upstroke, and a strong shock appears at around the same angle of attack. The boundary layer separates after the shock, and this results in trailing edge stall at α=10-12° depending on the oscillation amplitude. After separation, a highly unsteady flow with high lift remains, and reattachment is from the trailing edge with the supersonic regions near the leading edge being the last to reattach. The EDI-M112 follows this scheme too, but the shock is significantly stronger.

VARIATION OF FREQUENCY

The frequency was varied at constant amplitude, to separate the effects of varying $\overline{\alpha'}$ by $\alpha_{\pm}$ variation at constant f and by f variation at constant $\alpha_{\pm}$. Figures 9 and 10 illustrate the effect of varying the oscillation frequency for the EDI-M109 and EDI-M112 airfoils respectively. For both airfoils it can be seen that the lower frequencies have a stronger nonlinearity above α=11° than for higher frequencies. The higher frequencies also have a higher peak in lift and a lower lift in the separated part of the cycle. The effect of the frequency is strongest on the height of the pitching moment peak. The higher reduced frequencies increase the pitch-

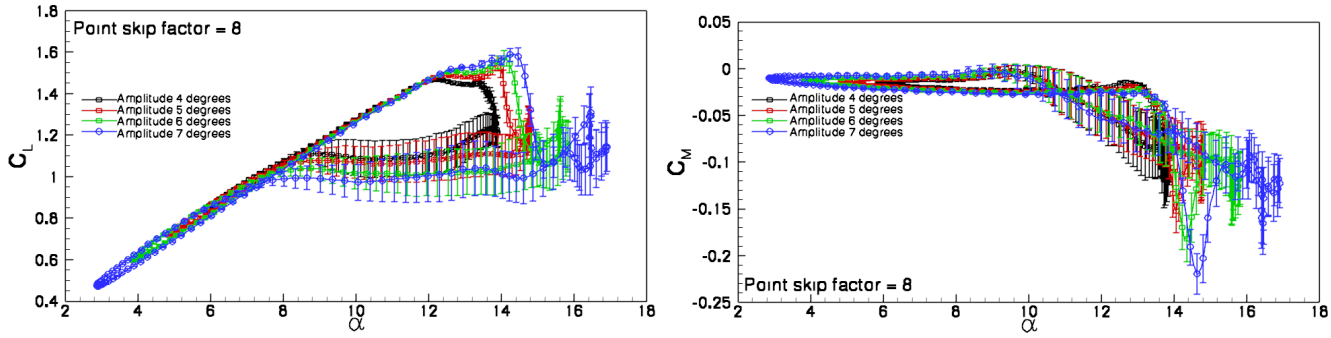

Figure 7: Comparison of lift (Left) and pitching moment coefficient (Right) for the EDI-M109 airfoil with various amplitudes at M=0.4, Re=2.4e6, f=6.6 Hz, α=10±4-7°.

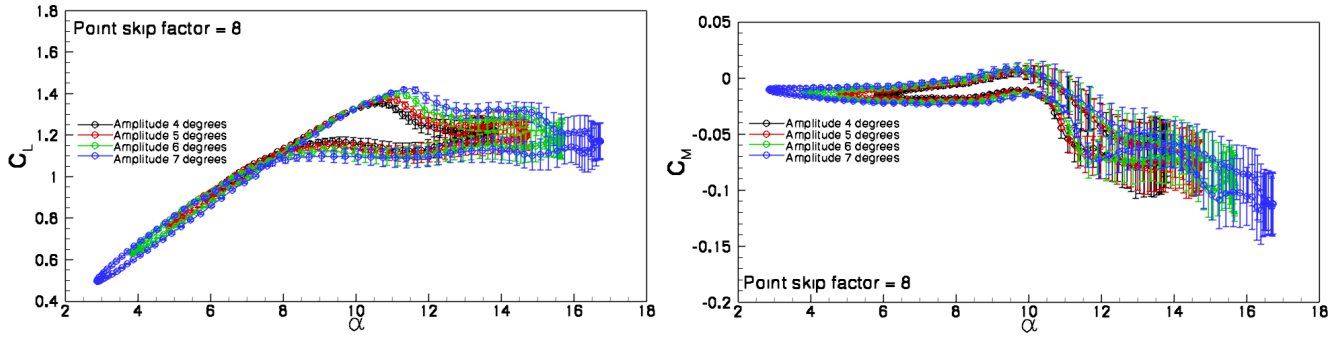

Figure 8: Comparison of lift (Left) and pitching moment coefficient (Right) for the EDI-M109 airfoil with various amplitudes at M=0.5, Re=3.0e6, f=6.6 Hz, α=10±4-7°.

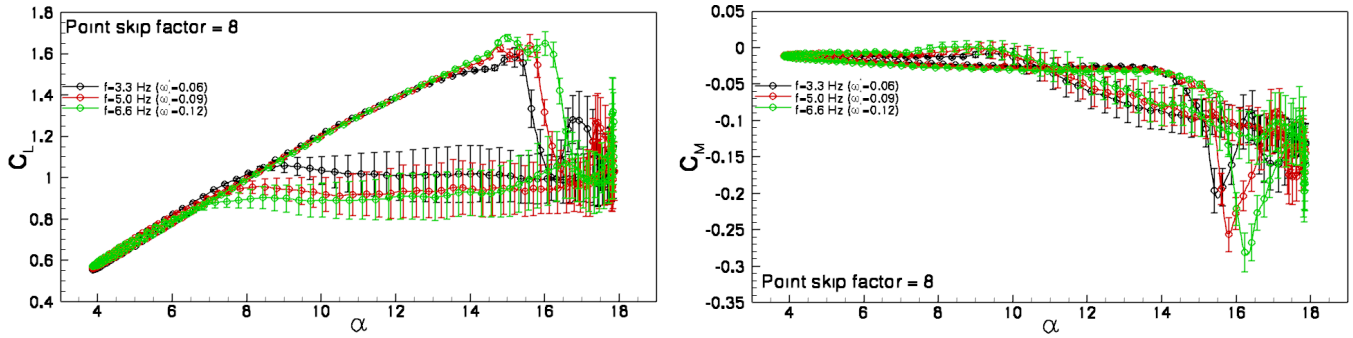

Figure 9: Comparison of lift (Left) and pitching moment coefficient (Right) for the EDI-M109 airfoil with various frequencies at M=0.3, Re=1.8e6, f=3.3, 5.0, 6.6 Hz, α=11±7°.

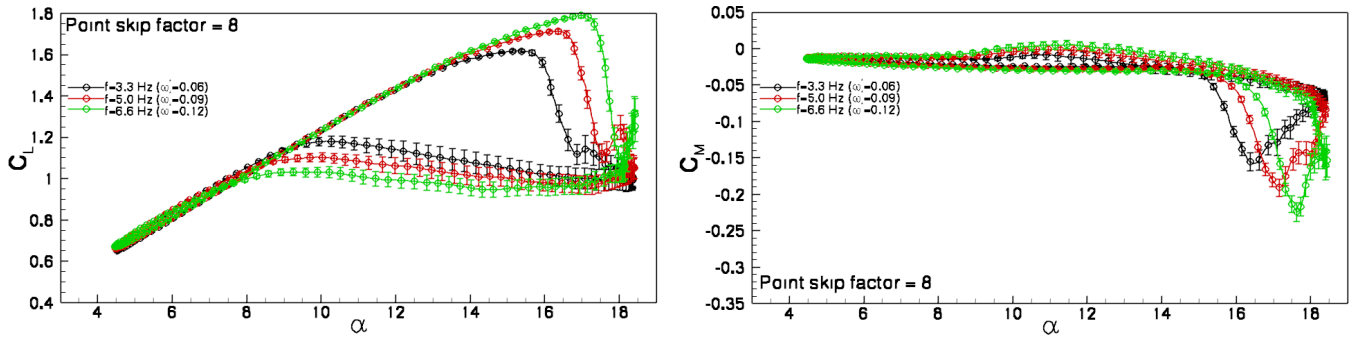

Figure 10: Comparison of lift (Left) and pitching moment coefficient (Right) for the EDI-M112 airfoil with various frequencies at M=0.3, Re=1.8e6, f=3.3, 5.0, 6.6 Hz, α=11±7°.

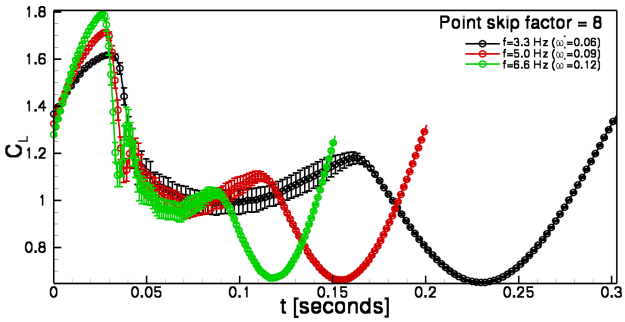

Figure 11: Lift coefficients from Figure 10 plotted against time.

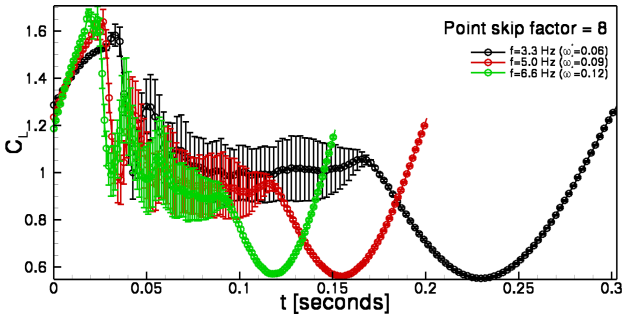

Figure 12: Lift coefficients from Figure 9 plotted against time.

ing moment peak significantly. Moving from ω^*=0.06 to ω^*=0.09 increases the peak height by 24% for the EDI-M109 and 21% for the EDI-M112, and increasing the frequency from ω^*=0.09 to ω^*=0.12 increases the peak height by 11% for the EDI-M109 and 18% for the EDI-M112.

For the EDI-M112 (Figure 10), the stall behaviour is unchanged with frequency, with a trailing edge separation starting at around α=13° and propagating forward. As seen in Figure 11, although the highest frequency results in the highest angle of attack before separation, the time between the start and end of separation is lower for ω^*=0.12 (18 ms) than for ω^*=0.06 (25 ms). For higher frequencies the reattachment is delayed to lower angles and the cycle-to-cycle variation in the lift is reduced during the detached flow phase. The reattachment is always from leading edge to trailing edge.

For the EDI-M109 (Figure 9), a drastic change in the separation takes place. Here at f=6.6 Hz leading edge separation is seen, similar to that in Figure 2, but at f=3.3 Hz trailing edge separation occurs. The boundary layer at the trailing edge begins to become unstable at α=13° for all cases, separating soon after, and then the separated region propagates forward. At f=6.6 Hz and f=5.0 Hz, a leading edge separation occurs before this can propagate to the leading edge, but for f=3.3 Hz, the time before separation is sufficient for the trailing edge separation to reach the leading edge and cause full separation of the airfoil. Due to the lower frequency, the time between the start of trailing edge separation and loss of lift is more than doubled (from 10 ms to 21 ms) for f=3.3 Hz over f=6.6 Hz (Figure 12). In all cases the reattachment is from trailing edge to leading edge with the suction peak being the last to reattach. The reattachment at f=3.3 Hz is at significantly higher α than the cases at higher frequency.

The dynamic stall peak in the pitching moment increases

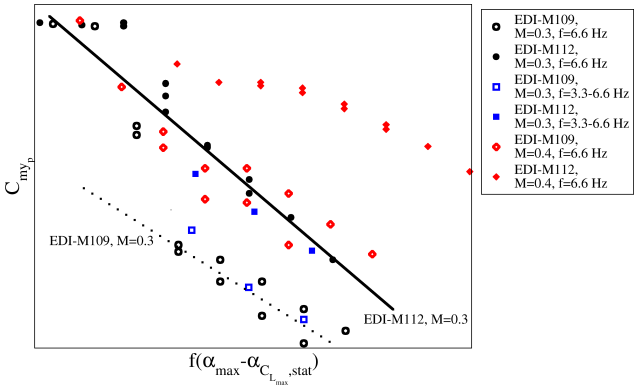

Figure 13: Relationship of C_{my_p} to normalised mean angular velocity $\overline{\alpha'_{norm}} = f(\alpha_{max} - \alpha_{C_{Lmax},stat})$ at Re/M=6×10^6 for varying amplitude, mean angle of attack and frequency.

with increasing amplitude, increasing mean angle of attack and with increasing frequency. If these values are combined as the normalised mean angular velocity:
$\overline{\alpha'_{norm}} = f(\alpha_{max} - \alpha_{C_{Lmax},stat})$,
where $\alpha_{C_{Lmax},stat}$ is the angle of attack at maximum lift for a static polar at these flow conditions and $\alpha_{max} = \overline{\alpha} + \alpha_{\pm}$, then an approximately linear relationship to peak pitching moment C_{my_p} can be seen. As seen in Figure 13, in this case, the data at varying amplitudes 4° $\leq \alpha_{\pm} \leq$8° and mean angle of attack 8° $\leq \alpha \leq$12° fall approximately onto a single line for each airfoil and Mach number for M=0.3 and M=0.4. The data at M=0.5 (not shown) also follows this schema. When normalised in this way, the data at M=0.3 with 3.3 Hz$\leq f \leq$6.6 Hz for both the EDI-M109 and EDI-M112 also falls approximately on a straight line, and this line is consistent with the data at varying amplitudes.

In order to test the idea in Figure 13 that the strength of the dynamic stall peaks is a function of the maximum angle of attack, cases were compared with the same maximum angle of attack and a different mean angle of attack at a constant pitching frequency. For light dynamic stall, where the maximum angle of attack of the airfoil is approximately equal to the angle of attack at separation, this results in similar dynamic stall qualities, and the dynamic stall strength is nearly independent of the minimum angle of attack. As the maximum angle of attack increases, the similarity is somewhat reduced.

At M=0.3 and Reynolds number 1.8e6, pitching with α=8°±7° and α=10°±5° give similar results (Figure 14), with a difference in C_{my_p} of 8% between the two cases shown. For the EDI-M112, pitching with α=8°±8°, α=10°±6° and α=12°±4° also gives similar results (Figure 15), with a difference in C_{my_p} of 1% between the three cases shown.

HIGHER ORDER PITCHING MOTION

The effect of higher order pitching motion on dynamic stall is interesting because the primary pitching motion of 1/rev for a helicopter blade is always overlaid with effects due to the elasticity of the blades. At conditions with dynamic stall the elasticity can have a significant effect on the local angle of attack of a section of blade. In order to partially simulate this, a dual-sine pitching motion of the type:

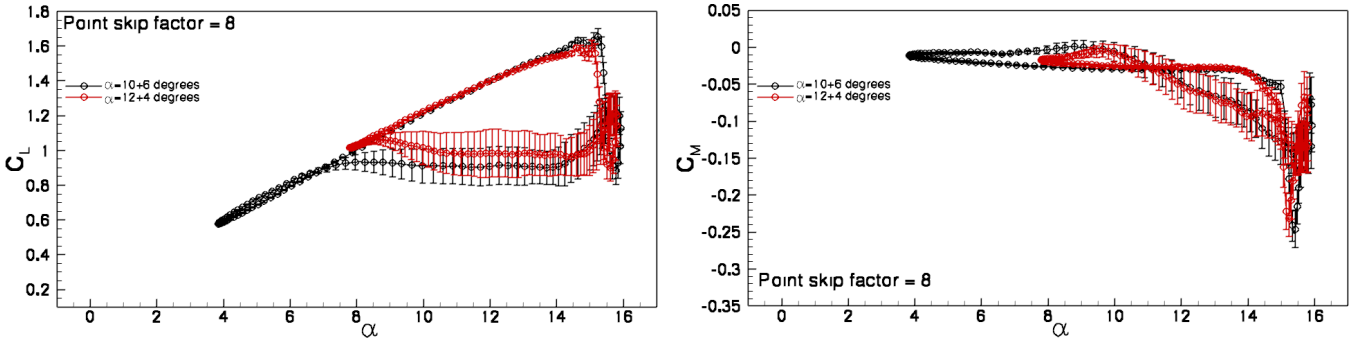

Figure 14: Comparison of lift (Left) and pitching moment coefficient (Right) for the EDI-M109 airfoil with constant maximum angle at M=0.3, Re=1.8e6, f=6.6 Hz, α=10±6°, 12±4°.

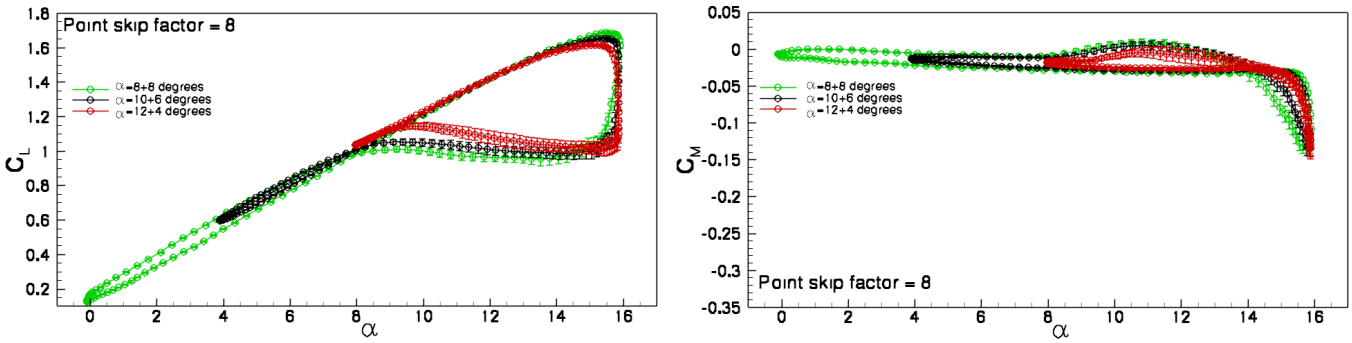

Figure 15: Comparison of lift (Left) and pitching moment coefficient (Right) for the EDI-M112 airfoil with constant maximum angle at M=0.3, Re=1.8e6, f=6.6 Hz, α=8±8°, 10±6°, 12±4°.

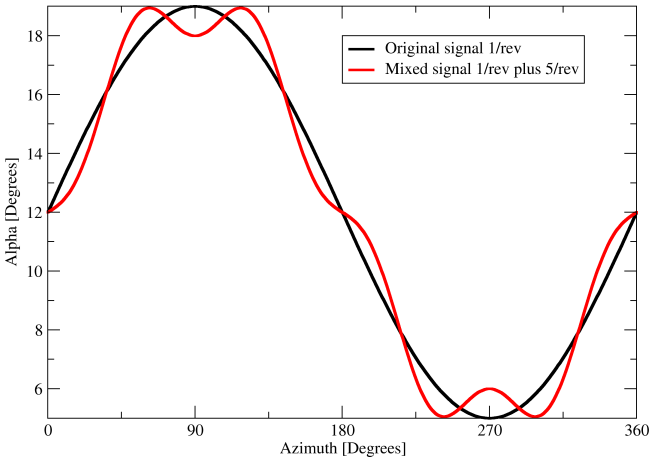

Figure 16: Comparison of the pitching motions.

$\alpha = 12° + 7° \sin(2\pi ft) + 1° \sin(5 \times (2\pi ft + \frac{\pi}{2}))$,
was generated and compared to a pitching motion of type:
$\alpha = 12° + 7° \sin(2\pi ft)$.
As seen in Figure 16, These pitching motions share the same maximum and minimum angles of attack, but have different shapes.

For the EDI-M109 (Figure 17) the additional higher frequency motion adds more wiggles into the lift curve, but qualitatively the result is the same. At α=12° on the upstroke, the 5/rev motion causes the upward movement to stop momentarily. This can be seen in Figure 17 by the more closely clustered symbols for the dual-sine case, where the time between two symbols is equal for the dual-sine and reference cases. The separation for the dual-sine case is at higher angle of attack, due to the higher angular velocity around the separation angle. The time between the end of the linear lift increase and the loss of lift is the same in both cases, but the higher angular velocity of the dual-sine case moves this time to a higher angle. The effect on the pitching moment peak is small, however, and well within the experimental uncertainty. For this case, it appears that using a dual-sine motion does not have any significant effect on the dynamic stall behaviour of the airfoil, so long as the maximum and minimum angles of attack remain constant.

For the EDI-M112 (Figure 18), the dual-sine case has more wiggles added into the lift curve, and in contrast with the results for the EDI-M109, the dual-sine case had significantly worse dynamic stall behaviour than for the simple sinusoidal pitching motion. The lift coefficients vary at α=12° on the upstroke, where the 5/rev motion causes the upward motion to stop momentarily. The increase in the lift and in the pitching moment for the dual-sine case has the same cause as seen for the EDI-M109. The two lift coefficients are nearly identical at α=15°, and from this point, the time to separation is the same (Figure 19), although the angle is different due to the higher angular velocity around the separation angle. The effect on the pitching moment peak is large, with a 35% increase in the pitching moment peak for the dual sine case over the simple sinusoidal motion.

Comparison of the Airfoils

A comparison of the dynamic properties of the airfoils provides a different suggestion about how far along the rotor the transition from the EDI-M109 to the EDI-M112 should be made than if the purely static polar data is used. Figure 20 shows a comparison between the EDI-M109, EDI-M112 and the OA209 airfoil measured at M=0.3 in the TWG. For the 2003 measurement of the OA209 airfoil,

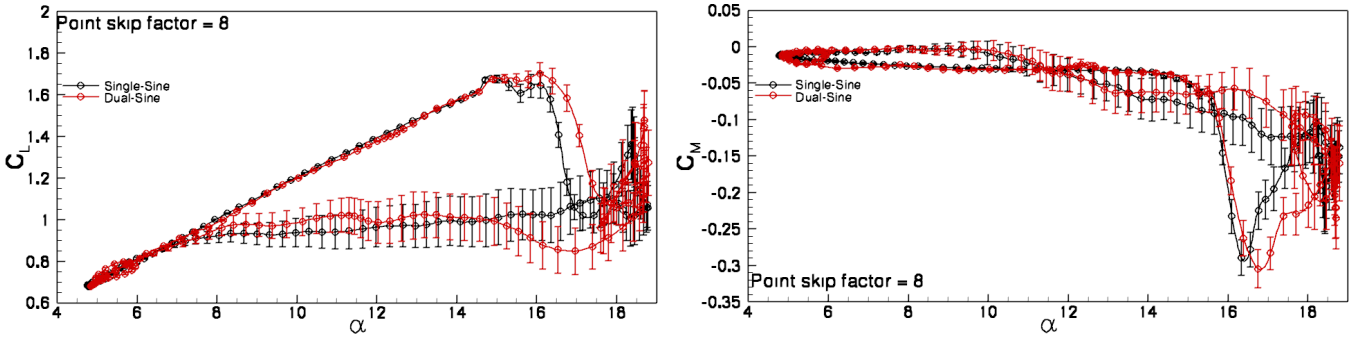

Figure 17: Comparison of lift (Left) and pitching moment coefficient (Right) for the EDI-M109 airfoil with single and dual-sine pitching motion at M=0.3, Re=1.8e6, f=6.6 Hz, α=12±7°.

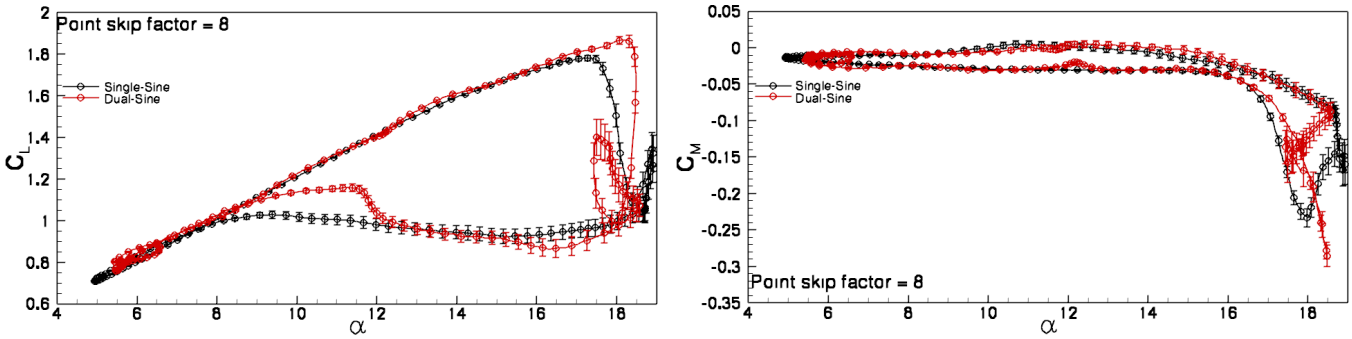

Figure 18: Comparison of lift (Left) and pitching moment coefficient (Right) for the EDI-M112 airfoil with single and dual-sine pitching motion at M=0.3, Re=1.8e6, f=6.6 Hz, α=12±7°.

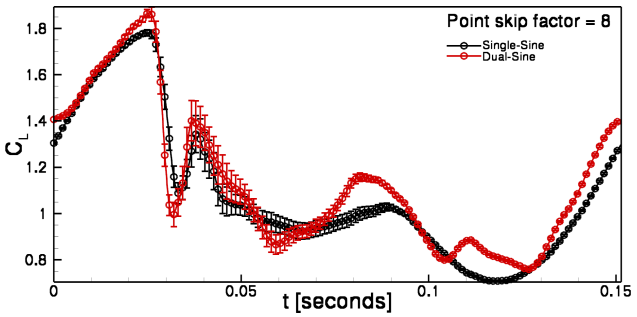

Figure 19: Lift coefficients from Figure 18 plotted against time.

data was sampled at 128 points per period instead the 1024 points used for the new tests. The OA209 airfoil, developed in the 1960s, is provided as a reference since the geometry is openly available. The OA209 model was not stiff enough for the high dynamic pressures used with the EDI airfoils, so the EDI airfoils were tested for one point which has been extensively investigated by the DLR as the DS2 test case [1, 5].

At M=0.3 the EDI-M109 has a significant improvement in mean lift and a reduction in the pitching moment peak, when compared to the OA209 at this test point (Figure 20). The advantage of the EDI-M112 over the OA209 is larger at this test point, with the pitching moment peak halved, and the lift increased over the EDI-M109. The change when the boundary layer transition reaches the leading edge and the slope of the lift curve reduces is visible in a divergence of the lift curves during the upstroke. At α=10° the lift of both airfoils has the same gradient and both airfoils have transition moving forward on the top surface. At α=14° the lift of both airfoils has the same gradient and both airfoils have transition at the leading edge. Between these points, the transition on the EDI-M109 reaches the leading edge at around α=11° and for the EDI-M112 the transition reaches the leading edge at around α=12°. The increased cycle-to-cycle variation in the flow after stall (leading to increased vibration) is up to twice as large for the OA209 as for the EDI-M112, and 3.5 times as large for the EDI-M109 as for the EDI-M112.

At M=0.4 (Figure 21) the advantage of the EDI-M112 over the EDI-M109 increases, since the EDI-M112 has a soft trailing edge stall with a relatively small pitching moment peak, where the EDI-M109 has a leading edge stall with a pitching moment peak nearly as big as that found for the OA209. For this case the lift curves in the upstroke are parallel and the boundary layer transition reaches the leading edge for both cases at around α=11°.

As seen in Table 2, the EDI-M112 is a better airfoil than the EDI-M109 for dynamic stall conditions at M=0.3 and M=0.4 and has a significantly higher (34-64%) mean glide ratio (as computed by the pressure taps) over a pitching cycle. The peak in the pitching moment is smaller for the EDI-M112 than the EDI-M109 for M=0.3 and M=0.4 and the peaks in lift and drag coefficient are better (lift peak is increased, drag peak is reduced). The EDI-M112 always has positive aerodynamic damping, and the damping is mostly higher than for the EDI-M09. The EDI-M109 has slightly negative aerodynamic damping at M=0.3 and M=0.4 for the test cases α=10±4° and α=12±4°. The higher modes (2/rev-6/rev) had damping too small for significance, except when dual-sine motion was used, and an increase in the 5/rev damping was noted. At M=0.5 the decision is not so clear, as the performance ($\overline{C_L}/\overline{C_D}$) is still 22-43% better for the EDI-M112, but the dynamic stall peak (C_{my_p}) in the pitching moment is up to 22% stronger for the EDI-M112. Both airfoils have positive aerodynamic damping at M=0.5.

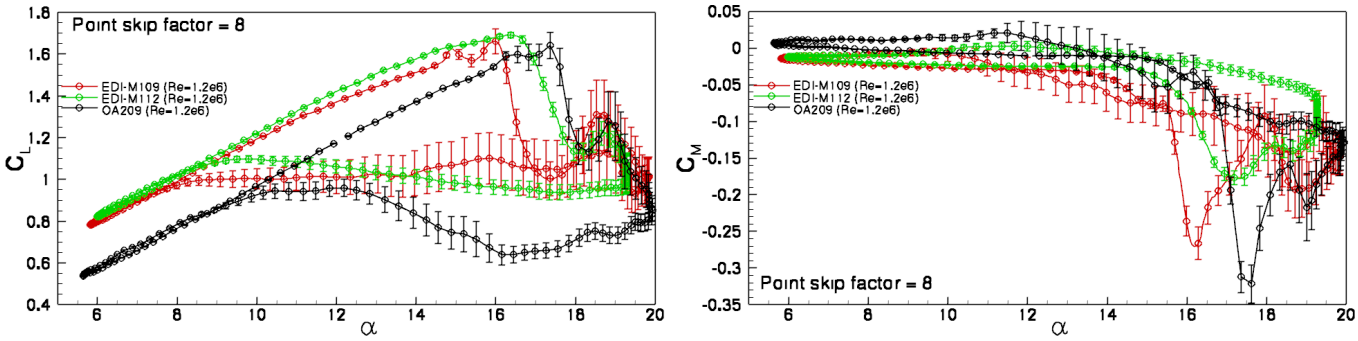

Figure 20: Comparison of lift (Left) and pitching moment coefficient (Right) for the EDI-M109, EDI-M112 and OA209 airfoils at M=0.31, Re=1.2e6, f=5.7 Hz, α=13±7°.

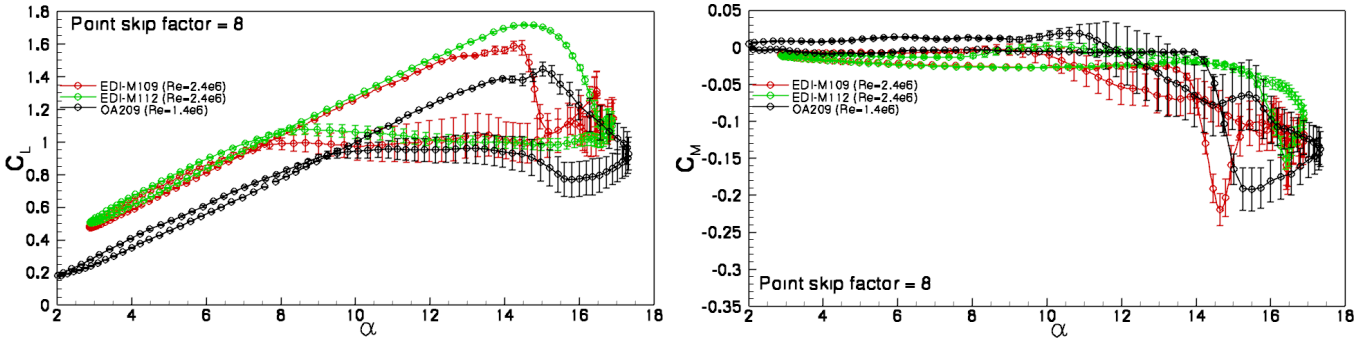

Figure 21: Comparison of lift (Left) and pitching moment coefficient (Right) for the EDI-M109, EDI-M112 and OA209 airfoils at M=0.4, Re=1.2e6 (OA209) or Re=2.4e6 (EDI-M109, EDI-M112), f=5.7 Hz, α=10±7°.

Based on this information, the dynamic pitching data suggests that the crossover point for the airfoil change between EDI-112 and EDI-M109 should be at between M=0.4 and M=0.5 on the retreating blade at maximum aircraft speed. The dynamic performance data suggests that the crossover should be at above M=0.5. Both of these indications may be different to the suggestion based on static airfoil polars.

LIIVA-CRITERION DAMPING

It has been posited by Liiva [4] that there is a correlation between low aerodynamic damping for high-frequency, low amplitude oscillations and poor unsteady aerodynamic performance, and Klein et al [3] suggest that these test cases indicate airfoils which will have a problem with higher order excitation of the blade. These low-amplitude cases would be particularly interesting for the airfoil design phase, because they potentially give a simple guideline to exclude a particular airfoil. A large number of these test cases were measured at $M \in$[0.3, 0.4, 0.5] and Re/M=6×10^6 and these are listed in Figure 22. Liiva's original experiments used excitation at a frequency corresponding to 6/rev, which would be 39.6 Hz for the EDI-series airfoils. Liiva used oscillation angles of $\alpha_\pm$=2.5° and $\alpha_\pm$=5.0° and noted changes in the damping coefficient of the model at higher angles of attack. These cases require $\overline{\alpha'}$=400°/sec and $\overline{\alpha'}$=800°/sec respectively, but due to the limitations of our pitching test rig, test points with $\overline{\alpha'} \leq$200°/second were considered. The frequency of the pitching motion was varied 13 Hz$\leq f \leq$45 Hz, the amplitude varied 0.5° $\leq \alpha_\pm \leq$2° and the mean angle of attack varied 12° $\leq \overline{\alpha} \leq$20°.

A comparison of the aerodynamic damping for both new airfoils for all test cases is shown in Figure 22. For M=0.3 at $\overline{\alpha}$=12°, the damping for both airfoils is positive and equal at $\alpha_\pm$=0.5° and $\alpha_\pm$=1.0°. At $\alpha_\pm$=2.0°, the damping for the EDI-M109 is suddenly negative, and clearly different than for the EDI-M112. At $\overline{\alpha}$=16°, the EDI-M112 generally has a slightly lower damping, and both airfoils show a strong tendency to lower damping at higher frequency. The cycle-to-cycle variation of the results is significantly increased compared to $\overline{\alpha}$=12°. At $\overline{\alpha}$=20°, the EDI-M112 again has a slightly lower damping than the EDI-M109, but the difference is small compared to the scatter of the data. No significant effect of amplitude or frequency on the damping is seen at $\overline{\alpha}$=20°. Since we know from the previous section that the EDI-M112 has better dynamic stall performance than the EDI-M109 at M=0.3, then the only data which supports this conclusion is at α=12±2°. Otherwise, no strong correlation is seen to the dynamic stall data.

At M=0.4, the points at $\overline{\alpha}$=16° and $\overline{\alpha}$=20° mostly overlap in the damping, and there is no significant effect of amplitude or frequency on the damping. At $\overline{\alpha}$=12° the results of the two airfoils is only significantly different at α=12±1°, where the EDI-M109 shows negative damping with damping increasing with increasing frequency. Since the data at both α=12±0.5° and α=12±2° show exactly the opposite tendency, it is difficult to say that a general correlation can be found between lower damping for the EDI-M109 at this case and the worse dynamic stall performance for the EDI-M109 at M=0.4 seen in the previous section. At M=0.5, no data could be taken at the highest angle of attack due to excessive model loads. At $\overline{\alpha}$=16° the data overlaps within the scatter, and at $\overline{\alpha}$=12° the EDI-M112 has a slight trend to lower damping.

The hypothesis that low aerodynamic damping of an airfoil with low amplitude, high frequency pitching motion is an indicator of poor dynamic stall performance is not supported by the experimental data. In contrast, the results for

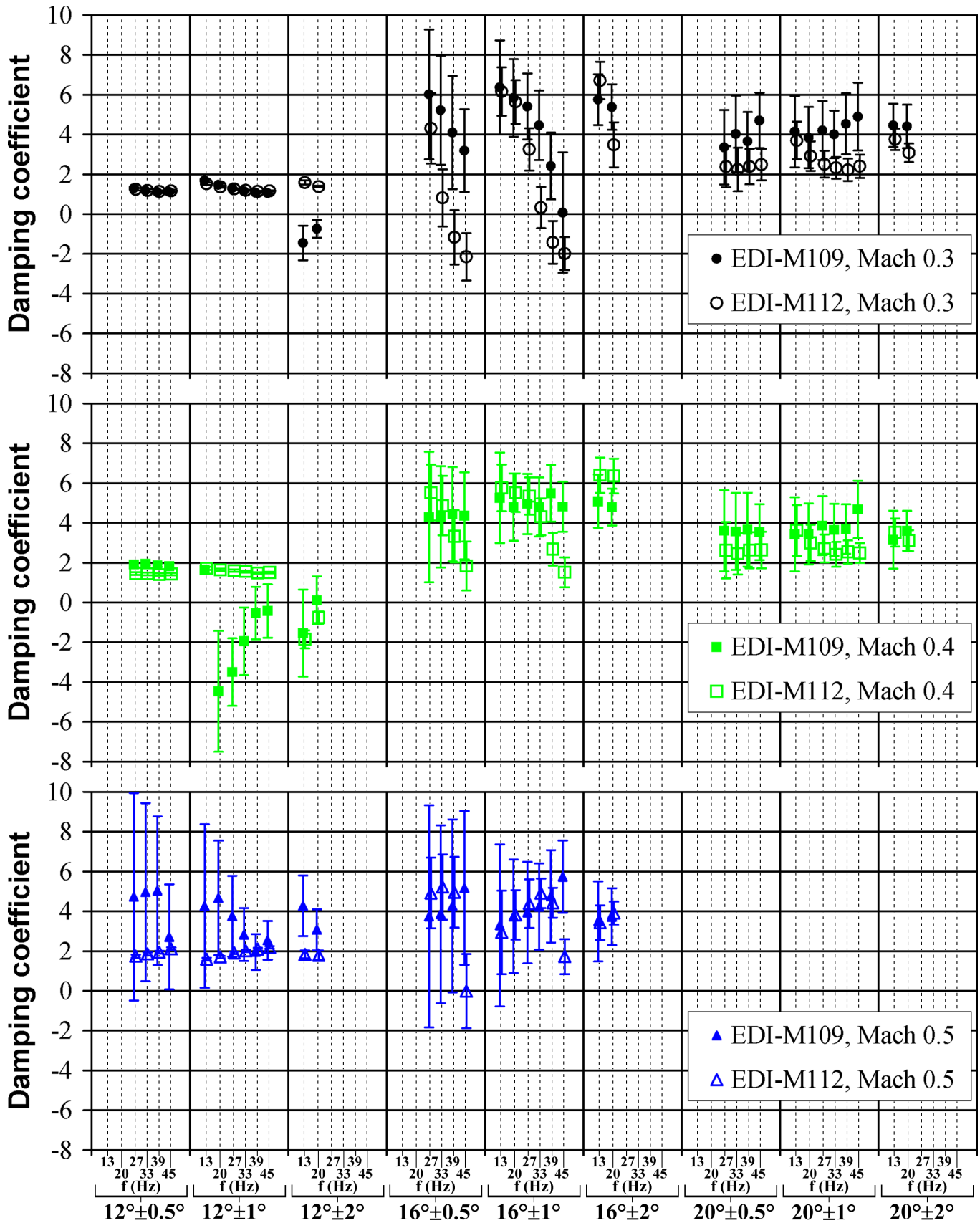

Figure 22: Overview of damping data at $Re/M=6\times10^6$ for the analysis of the airfoil using the Liiva criterion.

the two airfoils mostly lie within the scatter of the results, or is even in the opposite direction to that expected. The difference may be low because both of these airfoils have good dynamic stall performance, and a comparison with an airfoil with poor dynamic stall performance may give other results. Additionally the higher amplitudes at 6/rev originally applied by Liiva may give different results. The Liiva-criterion, as applied here, is not sensitive enough to distinguish between similar airfoils of a single design family within a design process and select a better airfoil for dynamic performance.

CONCLUSION

A high-quality dynamic aerodynamic test of two new airfoils has been carried out. The results are:

- The EDI-M109 and EDI-M112 airfoils have good dynamic performance, and an acceptable torsion peak, even for deep dynamic stall.
- The amplitude and frequency of the pitching motion was varied, and the strength of dynamic stall increased with increasing amplitude and frequency.
- The pitching moment peak size was found to have an approximately linear correlation to the normalised mean angular velocity $\overline{\alpha'_{norm}} = f(\alpha_{max} - \alpha_{C_{Lmax},stat})$. Test cases where the maximum angle of attack and oscillation frequency was preserved while varying amplitude had similar dynamic stall qualities.
- A mixture of 1/rev and 5/rev pitching motion changed the angular velocity at the separation angle, resulting in EDI-M109 performance qualitatively similar to that for pure 1/rev pitching and quite different EDI-M112 performance.
- The EDI-M112 is a better airfoil than the EDI-M109 for dynamic stall conditions at M=0.3 and M=0.4, with both better mean glide ratio and a smaller pitching moment peak. At M=0.5, the EDI-M112 still has a better mean glide ratio, but the pitching moment peak is higher than for the EDI-M109.
- No positive correlation was found between the aerodynamic damping at high-frequency, low amplitude oscillations, and the severity of dynamic stall. The Liiva-criterion, as applied here, is not sensitive enough to distinguish between similar airfoils of a single design family within a design process and select a better airfoil for dynamic performance.

Analysis of the experimental data is continuing (see also [2]), with a comparison with numerical results by the DLR in preparation. This includes a comparison of the dynamic movement of the boundary layer transition point between experiment and DLR-TAU computations using numerical transition modelling.

References

[1] Gardner, A.D., Richter, K., Rosemann, H., *Numerical Investigation of Air Jets for Dynamic Stall Control on the OA209 Airfoil*, 36th ERF, Paris, 7-9 Sept. 2010.

[2] Klein, A., Richter, K., Gardner, A.D., Altmikus, A.R.M., Lutz, T., Krämer, E., *Numerical comparison of dynamic stall for 2-D airfoils and an airfoil model in the DNW-TWG*, 37th ERF, Milan, 3-5 Sept. 2011.

[3] Klein, A., Richter, K., Altmikus, A., Lutz, T., Krämer, E., *Unsteady criteria for rotor blade airfoil design*, 35th ERF, Hamburg, 22-25 Sept. 2009.

[4] Liiva, J., *Unsteady aerodynamic and stall effects on helicopter rotor blade airfoil sections*, Journal of Aircraft, Vol. 6, No.1, 1969.

[5] Richter, K., Le Pape, A., Knopp, T., Costes, M., Gleize, V., Gardner, A.D.: Improved Two-Dimensional Dynamic Stall Prediction with Structured and Hybrid Numerical Methods. 65th AHS Forum, Grapevine (Texas) (2009).

α	$\alpha_\pm$	f	Comparison $\frac{abs(X_{M112}-X_{M109})}{abs(X_{M112})}$				
(°)	(°)	(Hz)	$\frac{\overline{C_L}}{\overline{C_D}}$	C_{L_p}	C_{D_p}	C_{my_p}	D
Comparison at M=0.3							
8	4	6.6	0.34	0.02	1.56	0.04	-0.11
8	5	6.6	0.40	0.03	1.64	0.04	-0.22
8	6	6.6	0.62	0.02	3.54	3.28	0.73
8	7	6.6	0.60	0.01	3.69	1.86	0.43
10	4	6.6	0.65	0.03	4.09	3.46	1.27
10	5	6.6	0.59	0.02	2.58	1.44	1.33
10	6	6.6	0.57	0.00	1.54	0.88	0.60
10	7	6.6	0.54	0.02	1.08	0.61	0.33
12	4	6.6	0.55	0.01	1.23	0.73	1.42
12	5	6.6	0.53	0.01	0.98	0.55	0.82
12	6	6.6	0.50	0.04	0.77	0.41	0.45
12	7	6.6	0.47	0.05	0.55	0.27	0.29
Comparison at M=0.4							
8	4	6.6	0.48	0.05	1.54	0.00	-0.30
8	5	6.6	0.64	0.07	3.29	2.28	0.64
8	6	6.6	0.53	0.09	0.92	0.16	-0.50
8	7	6.6	0.56	0.07	1.18	0.54	-0.25
10	4	6.6	0.52	0.09	0.47	-0.02	3.00
10	5	6.6	0.53	0.07	0.61	0.16	0.29
10	6	6.6	0.53	0.07	0.77	0.33	0.17
10	7	6.6	0.51	0.07	0.78	0.44	0.00
12	4	6.6	0.49	0.08	0.37	0.09	0.87
12	5	6.6	0.49	0.07	0.49	0.18	0.47
12	6	6.6	0.47	0.08	0.52	0.22	0.23
12	7	6.6	0.44	0.07	0.26	0.08	0.20
Comparison at M=0.5							
8	4	6.6	0.43	0.07	1.01	1.82	-0.64
8	5	6.6	0.42	0.07	0.57	0.28	-0.44
8	6	6.6	0.39	0.06	0.32	-0.10	-0.31
8	7	6.6	0.34	0.06	0.12	-0.22	0.00
10	4	6.6	0.40	0.08	0.28	-0.02	-0.41
10	5	6.6	0.36	0.07	0.13	-0.20	-0.13
10	6	6.6	0.31	0.07	0.10	-0.13	-0.09
10	7	6.6	0.26	0.07	0.04	-0.16	0.05
12	4	6.6	0.32	0.08	0.00	-0.20	-0.19
12	5	6.6	0.27	0.08	0.02	-0.15	-0.10
12	6	6.6	0.24	0.07	0.06	-0.05	0.03
12	7	6.6	0.22	0.07	0.07	0.01	0.10

Table 2: Comparison of the EDI-M109 and EDI-M112 for dynamic stall test cases at Re/M=6×10^6. Positive numbers indicate that the EDI-M112 was the better selection for that test point.